Investigating Cell-Particle Conjugate Orientations in a Microfluidic Channel to Ameliorate Impedance-based Signal Acquisition and Detection*

Brandon K. Ashley, Ishika Mukerji, and Umer Hassan, *Member, IEEE*

***Abstract*—Many biomedical experimental assays rely on cell-to- microparticle conjugation and their subsequent detection to quantify disease-related biomarkers. In this report, we investigated the effect of particle attachment position on a cell's surface to a signal acquired using impedance cytometry. We also present a novel configuration of independent coplanar microelectrodes positioned at the bottom and top of the microfluidic channel. In simulation results, our configuration accurately identifies different particle positions around the cell. We implemented a channel design with focusing regions between electrodes, and considered external factors around the channel such as polydimethylsiloxane (PDMS) interacting with the electric field and physical constraints of top electrodes placed farther away from the channel which improves detection accuracy.**

I. Introduction

Impedance cytometry is a versatile detection method for micro and nano-scale materials which has been utilized and improved upon for decades [1]. Extrapolating data from objects based on physical properties from an electric field in a microfluidic channel, impedance cytometry is already applied for single object counting and quantification [2]. This technique is also advantageous to fluorescence or optical detection methods due to nondestructive sample analysis and inexpensive, miniaturized equipment [3]. In disease detection, impedance cytometry can either directly measure the different electrical properties of cells [4] or use electrically sensitive micro or nanoparticles as agents targeting cells expressing pathophysiologic phenotypes. For the latter, common methods use antibody-coated, electrically sensitive particles to target cell surface receptors and form particle-cell conjugates [5]. The use of impedance cytometry with cell-particle conjugates is being studied or has applications for many diseases including cancer [6], [7], diabetes [8], sepsis [9], HIV [10], and more [11], [12].

One limitation with impedance cytometry includes maintaining constant object positions during detection. As the electric field strength has spatial variation between electrodes, deviations in object trajectories will significantly alter its signal and stifle accurate identification. Techniques such as hydrodynamic focusing can ensure objects flow consistently across the electric field [13], but this process cannot control for objects with complicated centers of mass, similar to cell-particle conjugates. While designs have been proposed to reinvent channel and detection geometries to capture object size and positions, the limitations of current microfabrication techniques makes many designs exceedingly laborious and impractical for low-cost use, and their orientation control remains inadequate [14]. For cell-particle conjugates, it is imperative to accurately identify the particle regardless of their orientation around the cell, using configurations realistic for current fabrication technology.

Here we propose a novel impedance cytometry apparatus and explore electrical signals for cells with 3 μm polystyrene (PS) particles attached at various orientations. The final design uses two sets of coplanar electrodes above and below the channel, with the top electrodes positioned at varying distances away from the channel to represent physical fabrication constraints. The simulation additionally includes the presence of PDMS encompassing the channel to represent an *in vitro* device more accurately, which to the best of our knowledge is a component explored in an impedance cytometry simulation for the first time. By using a unique top (TCE) and bottom coplanar electrodes (BCE) configuration and changing TCE height above the surrounding PDMS, this report explores to what degree particle-cell conjugates may be identified irrespective of particle attachment location.

II. Materials and Methods

A. Microfluidic architecture modeling

COMSOL Multiphysics 5.3a (Burlington, MA) was used to conduct the simulations. PDMS encases the microfluidic channel and is 1000 μm x 300 μm x 30 μm (Fig. 1a). The channel is filled with phosphate buffered saline (PBS) and is 1000 μm x 100 μm x 30 μm (Fig. 1b). Fig. 1a also shows 200 μm into the channel length starts the first of three gold electrodes on the channel floor, which are 100 μm x 300 μm x 0.5 μm, and spaced 150 μm apart. Additionally, there are focusing regions (FR) in the channel that reduces the width to 20 μm (Fig. 1b).

Significant material properties used for PDMS includes a 2.75 relative permittivity (ε_r) and $2.5\text{x}10^{-14}$ S/m electrical conductivity (σ) [15]. PBS had an ε_r of 80 and σ of 0.15 S/m [16], and gold had an $\boldsymbol{\varepsilon_r}$ of 1.6 and σ of $4.56\text{x}10^{6}$ S/m. Grounded electrodes were set to 0 V, the middle electrode was supplied a 10 V AC input at 300 kHz (Fig. 1a), and surface averaging over the grounded electrodes records the normalized

* Research supported by the National Institute of Health T32 GM135141 and the National Science Foundation Grant Number 2002511.

B.K. Ashley is with the Department of Biomedical Engineering at Rutgers, the State University of New Jersey, Piscataway, NJ 08854 USA.

I.M. is with the Department of Electrical Engineering at Rutgers, the State University of New Jersey, Piscataway, NJ 08854 USA.

U. Hassan is with the Department of Biomedical Engineering, the Department of Electrical Engineering, and the Global Health Institute at Rutgers, the State University of New Jersey, Piscataway, NJ 08854 USA (phone: 1-848-4452164, email: umer.hassan@rutgers.edu).

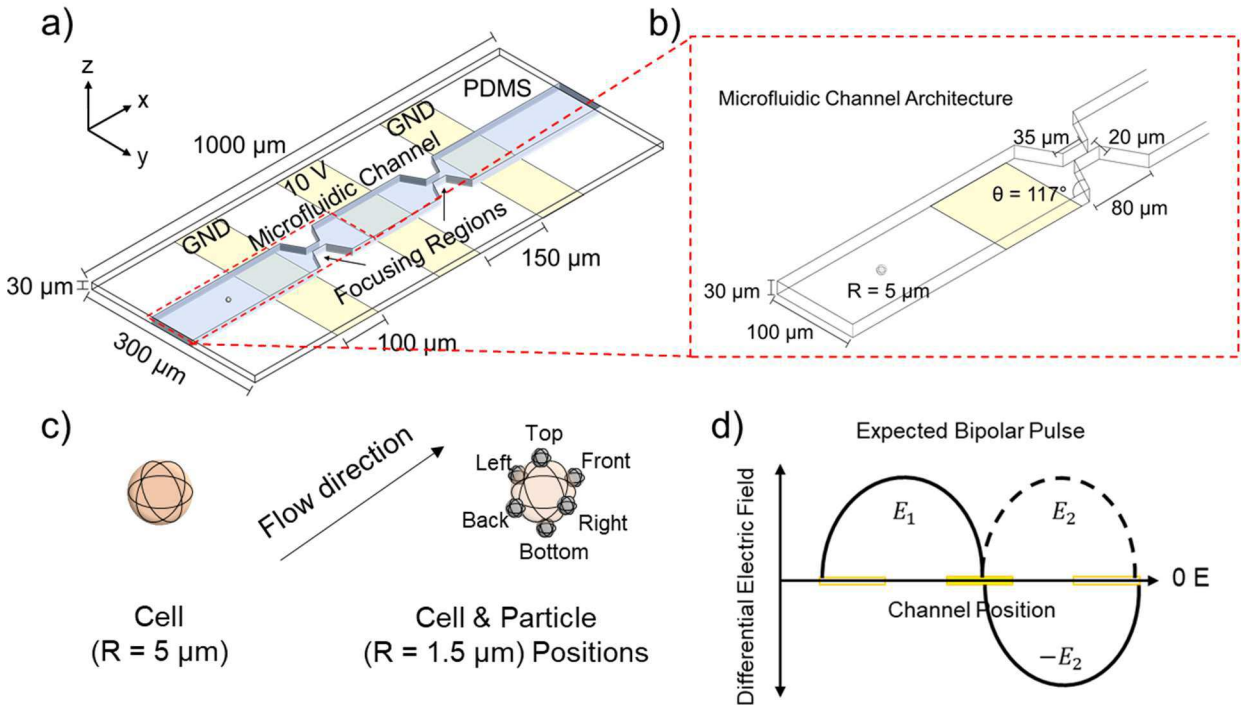

Figure 1. 3-D scheme for microsphere detection. a) Sensing region design, with a phosphate buffered saline (PBS) filled microfluidic channel (blue) encompassed by polydimethylsiloxane (PDMS). A 10 V input stimulates the middle gold (Au) electrodes with grounded outside coplanar electrodes. b) Expanded 3-D view of the microfluidic channel reveals focusing region dimensions. c) Immune cell (orange) with conjugated polystyrene particles (gray) with respective attachment orientations. d) Expected change as objects disrupt the electric field generated by the coplanar electrodes.

electric field changes.

B. Cell and particle modeling

A cell is modeled as a perfect sphere with a 5 µm radius, centered 15 µm above the channel base. Conjugated PS particles are also perfect spheres with a 1.5 µm radius, positioned on the surface of the cell either in the front, back, top, bottom, left, or right configurations (Fig. 1c). Samples are recorded with the cell and PS particles changing 'x' positions every 2 µm in channel length.

The cell has a ε_r of 50 and σ of 0.67 S/m, while PS particles have an ε_r of 2.6 and σ of 11.1 S/m. Convergence was solved after 4 iterations, and an 'Extra Fine' physics-controlled mesh was used.

C. Data processing and signal acquisition

Resistance differences between the cell/particles and the PBS in the channel alters the electric field generated as the cell/particle changes position. A differential signal is acquired after subtracting the second grounded electrode recordings from the first to form a bipolar pulse (Fig. 1d). When taking the peak-to-peak change, this total electric field change defines the final resulting signal value (Eq. 1):

$$\Delta E_T = \Delta E_{Max} - \Delta E_{Min} \quad (1)$$

This total ΔE (V/m) represents the object(s) in the electric field area as a function of both size and material properties. Another quantification includes the full width at half maximum (FWHM) value, which measures across what distance the object records at least half its maximum peak signal across the electric field (Eq. 2):

$$\text{FWHM} = \text{length(x) for } |\Delta E_x| \geq |\Delta E_T/2| \quad (2)$$

III. Results

A. Focusing region effects

The influence of FRs between electrodes was simulated to confirm their improved signal collection. Fig. 2a) affirms these results, as a larger bipolar pulse is realized when FRs are used from measuring the differential electric field between grounded electrodes (ΔE_T). A heatmap of the electric potential distribution in the channel for both with (Fig. b) and without FRs (Fig. 2c) shows a constricted gradient at the site of maximum peak collection; the midpoint of the grounded and active electrodes. A greater pulse amplitude results, while keeping background noise constant and improving the designs signal to noise ratio (SNR) from 41.6 to 52.2. For physical channels, this will also fix an object's position in the 'y' direction and reduce object-to-object positional variability.

B. Bottom coplanar electrode signals

Fig. 3 details electrical signals recorded using only BCE. Values for the cell alone (black dotted line) are compared to a cell with single PS particles attached at various positions; left (gray), right (red), back (purple), front (orange), top (green), and bottom (blue), which are pictured in Fig. 1c). Values recorded during the bottom pulse are enhanced in the Fig. 3 pop-out to better visualize differences between simulations.

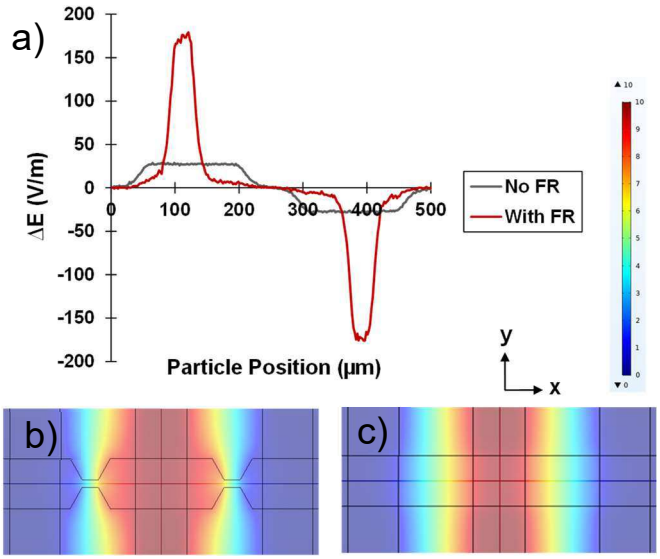

Figure 2. Differential electric field (ΔE) changes for a cell (radius = 5 μm) with focusing regions (FR, red) and without FR (gray). Top-down view of electric potential heat map with (b) and without FRs (c) from 0 (blue) to 10 (red) V.

With BCE electrodes alone, changes that arise from attached particles are miniscule as supported by the differential peak-to-peak signal (ΔE_T) and FWHM changes summarized in Table 1. However, trends are apparent, such as the bottom particle having the largest ΔE_T increase due to closer proximity to the bottom electrodes and displacing media in a stronger electric field (i.e., electric field strength decreases exponentially with increasing height in the z-direction). Additionally, particles attached equatorially (e.g., the front, back, left, and right particles) increased peak width shown by the FWHM changes, as particles at these positions extend the object's presence in the detection region. While a combination of signal amplitude and width can recognize particles at most positions, the particle attached on top of the cell yields the least metric contrast. Certainly, only a 1.4% change in ΔE_T and no change in FWHM, the top position does not extend the object's horizontal range, and is farthest from the BCE due to interacting with the weakest electric field. Using only BCE,

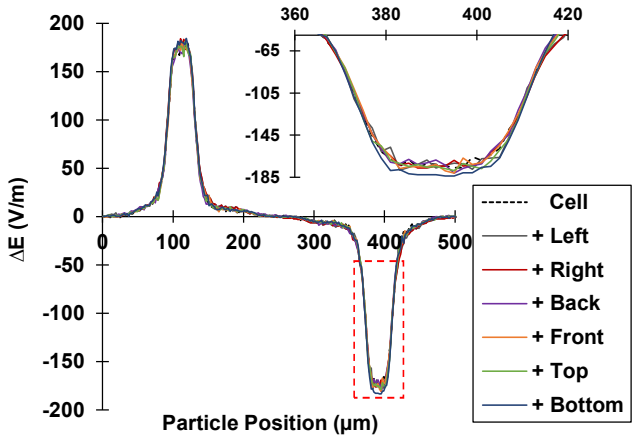

Figure 3. Differential electric field (ΔE) for a cell with conjugated particles at different orientations using BCE and enhanced pulse region to highlight differences.

TABLE I. PEAK SIGNAL RECORDINGS (ΔE_T) FROM BCE AND FULL-WIDTH HALF MAXIMUM (FWHM) FOR OBJECTS IN CHANNEL.

Object orientation	BCE ΔE_T (V/m)	FWHM (μm)	% ΔE_T change vs. cell	% FWHM change vs. cell
Cell	355	38.0	--	--
+ Front	361	39.5	1.69%	3.95%
+ Back	360	40.0	1.41%	5.26%
+ Left	358	41.5	0.85%	9.21%
+ Right	360	41.0	1.41%	7.89%
+ Top	360	38.0	1.41%	0%
+ Bottom	368	38.0	3.66%	0%

the design lacks sensitivity to sufficiently differentiate particles attached and entirely neglects the top particle.

C. Top-bottom electrode configuration

To improve overall sensitivity and provide ubiquitous coverage of particle attachment around the cell, the simulation introduces a series of independent top coplanar electrodes (TCE) with the same voltage input and grounded configuration (Fig. 4). The simulations start with TCE directly above the microfluidic channel (z_0), but signal strength is also investigated for TCE placed at various heights separated by PDMS layers (z_1–z_n). For quantification, the differential electric field values from both TCE and BCE are summed together (TBCE).

Fig. 5 reveals attached particle peaks vary more significantly using TBCE. Trends remain consistent to BCE experiments but are more pronounced, as particles attached equatorially saw greater FWHM widths and the bottom particle had the largest ΔE_T with over a 27% increase in bipolar signal (Table 2). TBCEs also allows the top position to be identified, as the change in ΔE_T is much greater from a more comprehensive electric field formed in the detection regime. Using the positions tested for and with TBCE, the changes in ΔE_T, FWHM, or a combination thereof allow signals that differentiate the object from a single cell with attached particles.

Studies were also conducted to investigate signal strength of the TCE alone as they are placed farther away from the channel above PDMS (Fig. 4). Fig. 6 shows that this signal falls off rapidly even a few microns away from the channel. While differences between the cell alone and with the top particle attached are more apparent as the electrodes are farther away (Fig. 6, % changes), the SNR is much lower, and

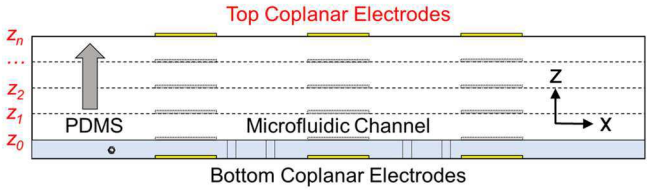

Figure 4. Cross-sectional scheme for microparticle detection with TBCE. Here, the PDMS height varies to explore dependencies related to electric field strength.

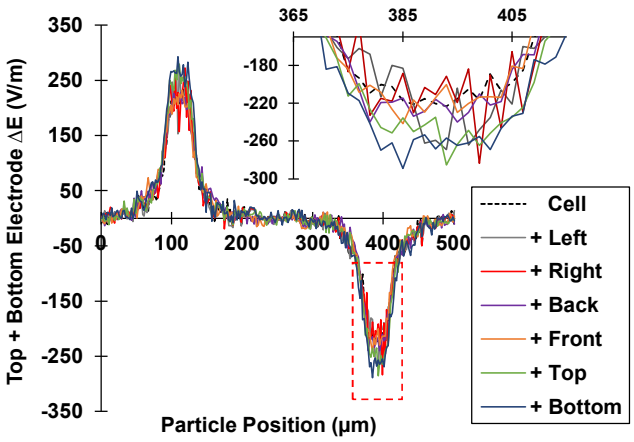

Figure 5. Differential electric field (ΔE) for a cell with conjugated particles at different orientations using TBCE and enhanced pulse region to highlight differences.

signal is harder to discern from noise. However, signals can still be differentiated and allows more opportunities for TCE fabrication methods.

IV. Conclusion

We have shown that signal changes for a 3 μm PS particle attached at different positions of a 10 μm cell, both by amplitude and signal width. The top particle position was especially weak using only BCE, so TCE were utilized and improved orientation detection. We also showed signal decays logarithmically as electrodes are farther from the channel but can still detect the top particle. Strategies for translating to a physical design include microfabricating the TCE directly above the cured PDMS. Going forward, future studies may evaluate its feasibility as well as cell position variance in the channel.

TABLE II. ΔE_T AND FWHM FROM TBCE (TCE + BCE SIGNAL) WITH TOP ELECTRODES 3 μM ABOVE CHANNEL.

Object orientation	TBCE ΔE_T (V/m)	FWHM (μm)	% ΔE_T change vs. cell	% FWHM change vs. cell
Cell	458	39.0	--	--
+ Front	473	42.5	1.69%	8.97%
+ Back	468	43.5	1.41%	11.54%
+ Left	548	40.0	19.65%	2.56%
+ Right	556	40.0	21.40%	2.56%
+ Top	564	38.5	23.14%	-1.28%
+ Bottom	582	41.0	27.07%	5.13%

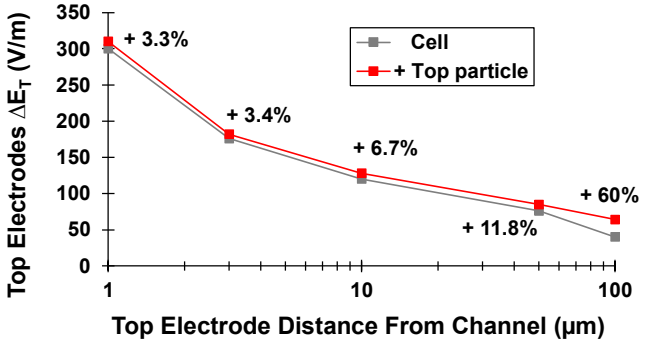

Figure 6. Semi-log plot of peak-to-peak amplitude (ΔET) recorded by top electrodes at different heights above the channel, with signal increasing (percentages) when the top particle (red) is attached vs. the cell alone (gray).

References

[1] W. H. Coulter, "Means for counting particles suspended in a fluid," US2656508A, Oct. 20, 1953

[2] D. Holmes and H. Morgan, "Single Cell Impedance Cytometry for Identification and Counting of CD4 T-Cells in Human Blood Using Impedance Labels," Anal. Chem., vol. 82, no. 4, pp. 1455–1461, Feb. 2010.

[3] B. K. Ashley and U. Hassan, "Point-of-critical-care diagnostics for sepsis enabled by multiplexed micro and nanosensing technologies," WIREs Nanomedicine and Nanobiotechnology, vol. n/a, no. n/a, p. e1701, Mar. 2021.

[4] U. Hassan et al., "A point-of-care microfluidic biochip for quantification of CD64 expression from whole blood for sepsis stratification," Nature Communications, vol. 8, no. 1, Art. no. 1, Jul. 2017.

[5] B. K. Ashley, J. Sui, M. Javanmard, and U. Hassan, "Functionalization of hybrid surface microparticles for in vitro cellular antigen classification," Anal Bioanal Chem, vol. 413, no. 2, pp. 555–564, Jan. 2021.

[6] T. Y. Lee, K.-A. Hyun, S.-I. Kim, and H.-I. Jung, "An integrated microfluidic chip for one-step isolation of circulating tumor cells," Sensors and Actuators B: Chemical, vol. 238, pp. 1144–1150, Jan. 2017.

[7] Z. Lin et al., "Rapid Assessment of Surface Markers on Cancer Cells Using Immuno-Magnetic Separation and Multi-frequency Impedance Cytometry for Targeted Therapy," Scientific Reports, vol. 10, no. 1, Art. no. 1, Feb. 2020.

[8] M. J. Sampson, I. R. Davies, S. Braschi, K. Ivory, and D. A. Hughes, "Increased expression of a scavenger receptor (CD36) in monocytes from subjects with Type 2 diabetes," Atherosclerosis, vol. 167, no. 1, pp. 129–134, Mar. 2003.

[9] S. Prakash, B. K. Ashley, P. S. Doyle, and U. Hassan, "Design of a Multiplexed Analyte Biosensor using Digital Barcoded Particles and Impedance Spectroscopy," Scientific Reports, vol. 10, no. 1, Art. no. 1, Apr. 2020.

[10] N. N. Watkins et al., "Microfluidic CD4+ and CD8+ T Lymphocyte Counters for Point-of-Care HIV Diagnostics Using Whole Blood," Science Translational Medicine, vol. 5, no. 214, pp. 214ra170-214ra170, Dec. 2013.

[11] S. Dellepiane, M. Marengo, and V. Cantaluppi, "Detrimental cross-talk between sepsis and acute kidney injury: new pathogenic mechanisms, early biomarkers and targeted therapies," Crit Care, vol. 20, no. 1, p. 61, Mar. 2016.

[12] Y. Pan et al., "Electrochemical immunosensor detection of urinary lactoferrin in clinical samples for urinary tract infection diagnosis," Biosensors and Bioelectronics, vol. 26, no. 2, pp. 649–654, Oct. 2010.

[13] N. Watkins, B. Murali Venkatesan, M. Toner, W. Rodriguez, and R. Bashir, "A robust electrical microcytometer with 3-dimensional hydrofocusing," Lab on a Chip, vol. 9, no. 22, pp. 3177–3184, 2009.

[14] H. Daguerre, M. Solsona, J. Cottet, M. Gauthier, P. Renaud, and A. Bolopion, "Positional dependence of particles and cells in microfluidic electrical impedance flow cytometry: origin, challenges and opportunities," Lab Chip, vol. 20, no. 20, pp. 3665–3689, Oct. 2020.

[15] A. S. M. Sayem, R. B. V. B. Simorangkir, K. P. Esselle, R. M. Hashmi, and H. Liu, "A Method to Develop Flexible Robust Optically Transparent Unidirectional Antennas Utilizing Pure Water, PDMS, and Transparent Conductive Mesh," IEEE Transactions on Antennas and Propagation, vol. 68, no. 10, pp. 6943–6952, Oct. 2020.

[16] D. G. Archer and P. Wang, "The Dielectric Constant of Water and Debye-Hückel Limiting Law Slopes," Journal of Physical and Chemical Reference Data, vol. 19, no. 2, pp. 371–411, Mar. 1990.